ACS APPLIED MATERIALS & INTERFACES

Research Article

www.acsami.org

A Facile in Situ Synthesis Route for $CuInS_2$ Quantum-Dots/In_2S_3 Co-Sensitized Photoanodes with High Photoelectric Performance

Yuan-qiang Wang,[†,§] Yi-chuan Rui,[‡] Qing-hong Zhang,[‡] Yao-gang Li,*[,‡] and Hong-zhi Wang*[,†]

[†]State Key Laboratory for Modification of Chemical Fibers and Polymer Materials, College of Materials Science and Engineering, Donghua University, Shanghai 201620, China

[‡]Engineering Research Center of Advanced Glasses Manufacturing Technology, MOE, Donghua University, Shanghai 201620, China

[§]College of Chemistry and Chemical Engineering, Shanghai University of Engineering Science, Shanghai 201620, China

ABSTRACT: $CuInS_2$ quantum-dot sensitized TiO_2 photoanodes with In_2S_3 buffer layer were in situ prepared via chemical bath deposition of In_2S_3, where the Cd-free In_2S_3 layer then reacted with TiO_2/Cu_xS which employed a facile SILAR process to deposit Cu_xS quantum dots on TiO_2 film, followed by a covering process with ZnS layer. Polysulfide electrolyte and Cu_2S on FTO glass counter electrode were used to provide higher photovoltaic performance of the constructed devices. The characteristics of the quantum dots sensitized solar cells were studied in more detail by optical measurements, photocurrent−voltage performance measurements, and impedance spectroscopy. On the basis of optimal Cu_xS SILAR cycles, the best photovoltaic performance with power conversion efficiency (η) of 1.62% (J_{sc} = 6.49 mA cm^{-2}, V_{oc} = 0.50 V, FF = 0.50) under full one-sun illumination was achieved by using Cu_2S counter electrode. Cu_2S-FTO electrode exhibits superior electrocatalytic ability for the polysulfide redox reactions relative to that of Pt-FTO electrode.

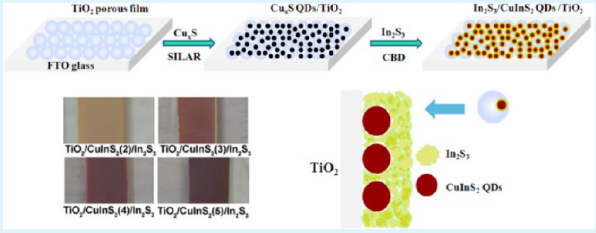

KEYWORDS: *$CuInS_2$, quantum-dot sensitized TiO_2 photoanodes, In_2S_3 buffer layer, Cu_xS quantum dots, Cu_2S counter electrode*

1. INTRODUCTION

Semiconductor quantum-dot sensitized solar cells (QDSSCs) have recently drawn significant attention since inorganic quantum dots (QDs) with narrow band gap and appropriate band positions are considered to be next generation alternative sensitizers of costly dyes in dye-sensitized solar cells (DSSCs).[1−8] Among various semiconductor materials used in solar cells, I−III−VI ternary semiconductor such as $CuInS_2$ is a very promising absorber for high-efficiency solar cells due to its befitting direct band gap, high absorption coefficient, low toxicity and long-term stability.[9−11] $CuInS_2$ sensitized solar cells have shown significant progress in recent years,[12−20] however the photovoltaic performance of $TiO_2/CuInS_2$-QDs photoanodes is still poor and the power conversion efficiency (PCE) is generally below 0.6%.[15,16,19,20]

To further improve the performance, the interface processes of charge carriers should be clearly understood. The performance for nanostructured solar cells is closely related to the interface processes. A better understanding of interfacial charge-transfer processes at TiO_2 film and QDs sensitizer or photoandode and counter electrode (CE) is important for the development of new strategies to improve the power conversion efficiency of QDSSCs. Cu_2S CE exhibited possible application as CE for QDSSCs by virtue of its high electrochemical catalytic activity reported by Hodes et al.[21] Approaches such as decreasing the charge recombination within the QDSSCs by modifying the blocking layer,[22] doping of CdS QDs with Mn^{2+} to improve the lifetime of trapped electron,[23] and a buffer layer on the interface of TiO_2 and $CuInS_2$-QDs sensitizer have been considered in this context. In $CuInS_2$-based solar cells, it has been revealed that unmatched band alignments and high surface state density existed in the heterostructure between TiO_2 and $CuInS_2$, which resulted in a high rate of recombination at the interface. Research has recently been focused on the interface modification of the TiO_2 and $CuInS_2$-QDs by applying a buffer layer such as CdS, CdSe, Cd-free Cu_2S, In_2S_3, and In_2Se_3, and those can suppress the interface electron recombination so that the cell performance can improved. For instance, both Teng et al.[16] and Kamat et al.[18] used saturation adsorption of $CuInS_2$-QDs solution and a CdS buffer layer to achieve PCEs of 4.2% and 3.91%, respectively. Similarly, Hu et al.[19] used heat treatment and CdS buffer layer to gain a PCE of 1.47%. Chang and co-workers[20] adopted Cu_2S, Cu_2Se, In_2S_3, In_2Se_3, CdS, or CdSe as buffer layer, and the PCEs are 0.58%, 1.06%, 1.22%, 0.89%, 1.35%, 2.55%, and 4.55% for $TiO_2/CuInS_2$, $TiO_2/Cu_2S/CuInS_2$, $TiO_2/Cu_2Se/CuInS_2$, $TiO_2/In_2S_3/CuInS_2$, $TiO_2/In_2Se_3/CuInS_2$, TiO_2/CdS/$CuInS_2$, and TiO_2/CdSe/$CuInS_2$ configurations, respectively. Though CdS or CdSe can provide the higher PCE for $CuInS_2$ co-sensitized solar cells, their toxicity may limit the further application for large-scale production.

Up to now, the reports on $CuInS_2$-based photoanodes have exploited two common methods: ex situ preparation of $CuInS_2$-

Received: August 22, 2013
Accepted: October 25, 2013
Published: October 25, 2013

QDs solution and in situ preparation containing copper, indium, and sulfur precursor solution. The first method uses chemical technology to presynthesize colloidal $CuInS_2$ QDs.[24−26] Then the QDs were anchored onto TiO_2 electrodes by means of bifunctional linker molecules containing carboxylic acid and thiol groups or direct adsorption.[13,16−19,22,27−30] This process can take advantage of the colloidal syntheses to control the growth dynamics, particle size, and crystal structure but may suffer from rather low QDs loading, high preparation cost due to expensive organic solvents, and relatively weaker electronic coupling between TiO_2 and QDs. Another approach utilizes the in situ preparation of $CuInS_2$ nanocrystal onto TiO_2 with the precursor solution by chemical spray pyrolysis (CSP),[31] spin-coating,[12] or successive ionic layer adsorption and reaction (SILAR).[14,15] The as-deposited $CuInS_2$ sensitized photoanodes with in situ method have high surface coverage of QDs; however, it usually involves high temperature vulcanizing process (450−500 °C) in order to increase the $CuInS_2$ crystallinity, which is considered to be an obstacle for the large-scale profitable operation and the fabrication of solar cells. Therefore, it is still desirable to develop novel methods to prepare $CuInS_2$ sensitized photoanodes and solve interface problems for the solar cell.

Herein, for the first time, we describe QD-sensitized solar cells consisting of $CuInS_2$-QDs sensitizer with Cd-free In_2S_3 buffer layer based on chemical bath deposition (CBD) of In_2S_3 and in situ reaction with TiO_2/Cu_xS-QDs films,; the overall strategy is presented in Scheme 1. The growth process of

Scheme 1. Schematic Processes for Preparing $CuInS_2$-QDs/In_2S_3 Anchored TiO_2 Porous Film on FTO Glass[a]

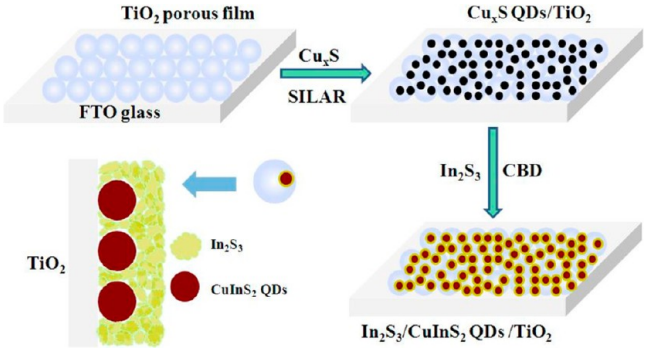

[a] Cu_xS-QDs grown on TiO_2 film with SILAR method, followed by $CuInS_2$-QDs/In_2S_3 on TiO_2 film based on CBD of In_2S_3 and reaction with TiO_2/Cu_xS-QDs film. The inset illustrates a conceptual schematic of the $CuInS_2$-QDs/In_2S_3 on the TiO_2 surface.

$CuInS_2$-QDs/In_2S_3 on TiO_2 film was demonstrated in detail. By using the Cu_2S CE and polysulfide electrolyte to assemble a QDSSC, the $CuInS_2$-QDs/In_2S_3 co-sensitizer provides a power conversion efficiency efficiency of 1.62% under one-sun illumination.

2. EXPERIMENTAL SECTION

2.1. Materials. Copper(II) acetate ($Cu(OAc)_2{\cdot}H_2O$, 99+%), sodium sulfide ($Na_2S{\cdot}9H_2O$, 98+%), indium chloride ($InCl_3{\cdot}4H_2O$, 98+%), thioacetamide (CH_3CSNH_2, 98+%), citric acid ($C_6H_8O_7{\cdot}H_2O$, 98+%), ethanol (99.5%), zinc acetate ($Zn(OAc)_2{\cdot}2H_2O$, 99+%), sulfur (S, 99.5%), and potassium chloride (KCl, 99.5%) were purchased from Sinopharm Chemical Reagent Co. (Shanghai, China). TiO_2 powder (P25, a mixed phase of 70% anatase and 30% rutile; average size 25 nm +) from Degussa (Japan) was used to prepare TiO_2 anatase nanoparticles for photoelectrodes. Ethylcellulose and terpineol from Fluka (Germany) were used to suspend TiO_2 particles in viscous solutions. All the materials were used without further purification. Fluorine-doped tin oxide (FTO) conducting glass substrate (2.3 mm thick, 14 Ω/□) was purchased from Nippon Sheet Glass.

2.2. Preparation of TiO_2/Cu_xS-QDs Electrodes. Mesoporous TiO_2 electrodes were prepared by following a method reported earlier.[32,33] In brief, FTO glass was cleaned in a detergent solution using an ultrasonic bath for 15 min and then rinsed with water and ethanol. Two layers of TiO_2 were deposited on FTO, a blocking layer and active layer. The blocking layer was deposited by treating the glass in a 40 mM $TiCl_4$ aqueous solution at 70 °C for 30 min followed by annealing at 500 °C for 30 min. The active TiO_2 layer (P25 paste) was coated on top of the blocking layer by the doctor blade technique. The film was dried at 125 °C for 6 min followed by annealing 500 °C for another 30 min. A post-treatment process of the calcined film was similar with that of blocking layer. The thickness of the TiO_2 mesoporous electrode was approximately 10 μm, measured by anoptical profiler (Wyko NT9100, Veeco Co., USA). TiO_2/Cu_xS-QDs electrodes were subsequently prepared by SILAR. The electrode was dipped into 0.05 M $Cu(OAc)_2$ aqueous solution for 30 s, rinsing with water, and subsequent 30 s immersion in 0.05 M Na_2S aqueous solution followed by further rinsing with water. Each series of two immersions was considered as one SILAR cycle.

2.3. Fabrication of the $CuInS_2$-QDs/In_2S_3/ZnS QDSSCs. QD-sensitized solar cells consisting of $CuInS_2$-QDs sensitizer with In_2S_3 buffer layer were prepared by CBD of In_2S_3 and in situ reaction with TiO_2/Cu_xS-QDs films with a one-step method. A precursor solution of $In_2S_3$was prepared from a mixture of $InCl_3$(0.01 M), CH_3CSNH_2 (0.04 M), and ethanol solution. During the mixing procedure, $C_6H_8O_7$ (0.06 M) was added with the chemical solution for the formation of indium complex. The resulting clear mixture was transferred into a 70 mL Teflon-lined stainless steel autoclave, holding a vertically oriented FTO glass substrate (with a Cu_xS/TiO_2 film), which was then sealed and maintained at 150 °C for 3 h. The substrate was then rinsed with water and ethanol and dried at room temperature. The electrode was marked as $TiO_2/CuInS_2(n)$-QDs/In_2S_3 according to the different Cu_xS SILAR cycle (where n is Cu_xS SILAR cycle). All the electrodes analyzed in this study have been coated with ZnS, carried out by two SILAR cycles consisting of twice dipping alternatively in the 0.1 M $Zn(OAc)_2$ and 0.1 M Na_2S aqueous solution for 1 min per dip. The QDSSCs were sealed in a sandwich structure with a spacer film (50 μm thick polyester film, DuPont) by using Pt-coated FTO glass[32,33] or Cu_2S-coated FTO glass as the CE. The Cu_2S-FTO glass CE was prepared by a modified method.[34,35]A droplet of an aqueous polysulfide solution containing 1 M Na_2S and 1 M S was added onto thin Cu-sputtered FTO glass causing it to suddenly become black, indicating the formation of Cu_2S. The space between the electrodes was filled with the polysulfide electrolyte which consisted of Na_2S (2 M), S (2 M), and KCl (0.2 M), using pure water as solvent. A mask with a window of 0.25 cm^2 was clipped on the photoanode side to define the active area of the cell.

2.4. Measurements. Transmission electron microscopy (TEM) images and high-resolution transmission electron microscopy (HRTEM) images were obtained using a JEM 2100 F (JEOL Co., Japan) operating at 200 kV. The surface morphology and structure of the resulting films was studied using a field emission scanning electron microscope (FESEM, S-4800, Hitachi, Japan) with energy dispersed X-ray spectrum (EDX, 10.0 kV). The crystal structure was investigated by an X-ray diffraction technique (XRD, D/max 2550 V, Rigaku, Japan) with Cu Kα (λ = 0.154 nm) radiation at 40 kV and 200 mA in 2θ ranging from 20° to 80°. UV-visible absorption spectra were recorded using a spectrophotometer (Lambda 950, Perkin-Elmer Co., USA). Photocurrent−voltage characteristics (J−V curves) of QDSSCs were measured using a Keithley 2400 Source Meter under illumination of simulated sunlight (100 mW cm^{-2}) provided by a Newport solar simulator (Model 96160) with an AM 1.5G filter. Impedance spectroscopy was performed using an electrochemical analyzer (Zahner-elecktrik GmbH & Co., Germany). Impedance measurements were carried out by applying a DC bias at open circuit voltage and an

AC voltage with an amplitude of 10 mV in a frequency range from 100 mHz to 100 kHz in the dark. The obtained spectra were fitted with Z-View software.

3. RESULTS AND DISCUSSION

3.1. Fabrication of $CuInS_2$-QDs/In_2S_3 Sensitized TiO_2 Photoanodes. Transmission electronic microscopy (TEM) images give direct evidence to estimate the coverage of QDs over the TiO_2 film electrodes. In the control experiment, plain TiO_2 film was also prepared (Figure 1a) and shows well-connected TiO_2 nanoparticles and their clean bare sufaces with average particle size of around ~30 nm as reported by a commercial source. Figure 1b shows the image of the prepared $CuInS_2$-QDs/In_2S_3 co-sensitized TiO_2 photoanode. From the image, the TiO_2 nanoparticle appears to be covered densely by smaller sensitizers ($CuInS_2$-QDs/In_2S_3), and the sensitizers sufficiently cover the nanocrystalline TiO_2 network with a thickness of 5−10 nm, which can be more clearly seen at the edge side of the TiO_2 nanoparticles. The high-resolution TEM (HRTEM) image of the TiO_2/$CuInS_2$-QDs/In_2S_3 composite (Figure 1c) clearly depicts the crystalline lattice fringes of the involved species. The lattice spacing distance of 0.352 nm, illustrated in the right zone of the image, corresponds to the (101) plane of anatase TiO_2. The lattices with spacing distances of 0.320 and 0.325 nm round TiO_2 particle correspond to the (112) plane of the $CuInS_2$ and (311) plane of the In_2S_3, respectively. The In_2S_3 coating with CBD method is in close contact with both the $CuInS_2$ QDs and TiO_2 particles.

$CuInS_2$-QDs/In_2S_3 sensitized TiO_2photoanodes were prepared based on chemical bath deposition of In_2S_3 and reaction with TiO_2/Cu_xS-QDs films. The whole reactions are

$$Cu^{2+} + S^{2-} \rightarrow Cu_xS$$

(The reaction was processed on TiO_2 films) (1)

$$SC(NH_2)_2 + C_2H_2OH \rightarrow H_2S + CO_2 + NH_3 \quad (2)$$

$$H_2S \rightleftarrows HS^- + H^+ \rightleftarrows S^{2-} + 2H^+ \quad (3)$$

$$L \rightleftarrows L^- + H^+ \text{ (L is citric acid)} \quad (4)$$

$$In^{3+} + L^- \rightleftarrows InL_3 \quad (5)$$

$$In^{3+} + S^{2-} \rightarrow In_2S_3 \quad (6)$$

$$Cu_xS + In_2S_3 \rightarrow CuInS_2 \quad (7)$$

The copper−sulfur aqueous chemistry is complex, as several stable and metastable phases of varying stoichiometries exist between ideal compositions of Cu_2S and CuS.[36] The SILAR method was used to deposit Cu_xS (x indicates the uncertain Cu and S mole ratio) on TiO_2 films as the basic electrode, and the growth mechanism of the Cu_xS-QDs on the TiO_2 films was monitored with FESEM images (see Figure 2a,b). It is clear that the entire surface of the FTO substrate is covered uniformly and densely with TiO_2 nanoparticles from Figure 2a. The average particle diameter is approximate 30 nm, and the average pore size among TiO_2 nanoparticles is less than 10 nm. After being assembled with Cu_xS for four cycles, the TiO_2 nanoparticles structure is retained, and the Cu_xS particles could be generated in the pores of porous TiO_2 films as shown in Figure 2b. Moreover, the pores have not been filled completely which can produce $CuInS_2$. In addition, the small diameter of pores of the TiO_2 films restricts further growth of the Cu_xS particles. Thus, Cu_xS particles were smaller in the porous TiO_2 films, meaning that the size of Cu_xS is in the scope of quantum dots. Figure 2c,d, shows the top view and cross-sectional FESEM images of the TiO_2/$CuInS_2$(4)-QDs/In_2S_3 photoanode. It was found that $CuInS_2$-QDs/In_2S_3 composites were in situ produced by CBD of In_2S_3 (the XRD pattern of In_2S_3 prepared by CBD method is shown in Figure 3a). The well-connected In_2S_3 layer-like nets were also found on the surface

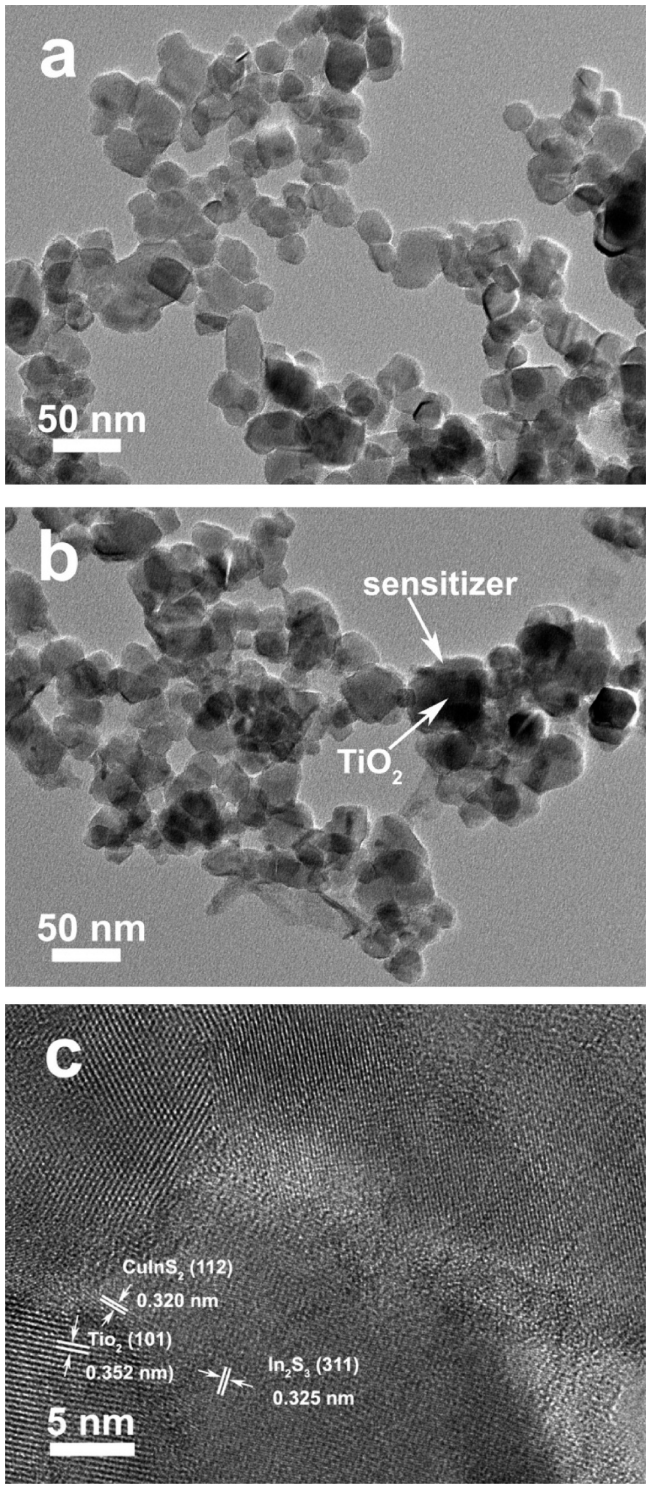

Figure 1. (a) TEM image of the plain TiO_2 film. (b) (c) TEM and the corresponding HRTEM image of TiO_2/$CuInS_2$(4)-QDs/In_2S_3 photoanode.

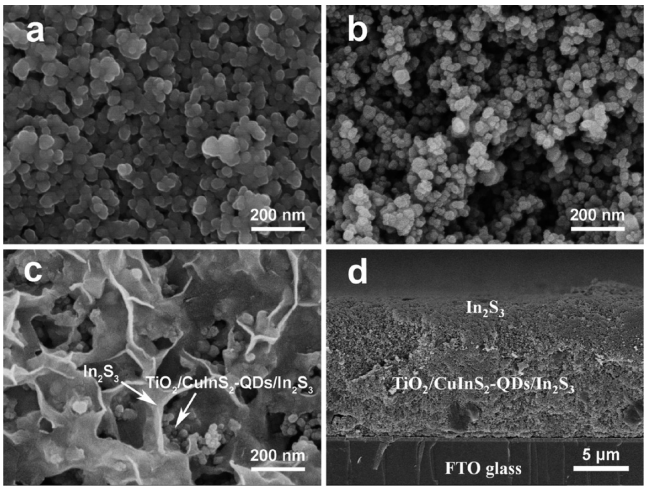

Figure 2. FESEM images of (a) plain TiO_2 film (top view). (b) TiO_2/Cu_xS-QDs electrode prepared by four cycles of Cu_xS SILAR deposition (top view). (c) and (d) are the top view and cross-sectional FESEM images of $TiO_2/CuInS_2(4)$-QDs/In_2S_3 photonaode.

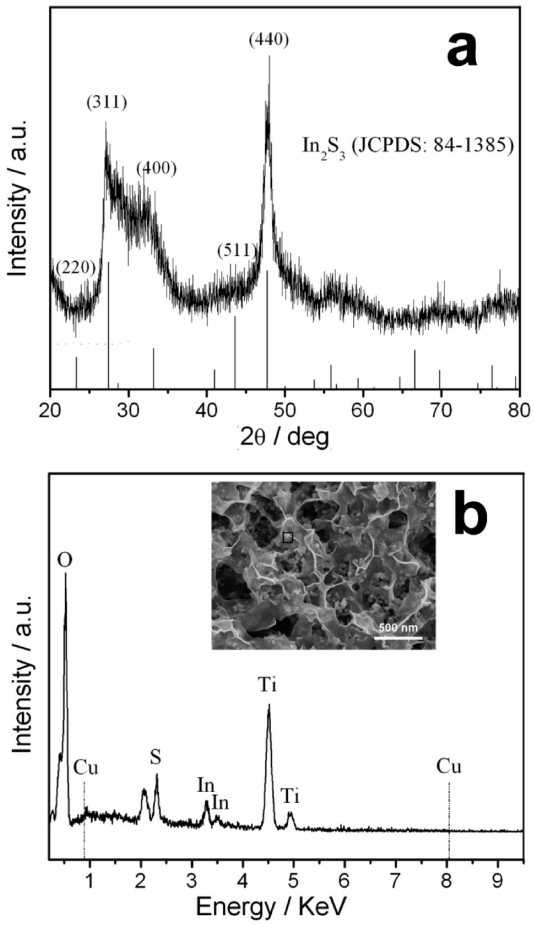

Figure 3. (a) XRD pattern of In_2S_3 prepared with the CBD method. (b) An EDX spectrum of the surface of $TiO_2/CuInS_2(4)$-QDs/In_2S_3 photonaode obtained by CBD of In_2S_3 and in situ reaction with TiO_2/Cu_xS-QDs film. The inset image is a high magnification FESEM image (top view) of $TiO_2/CuInS_2(4)$-QDs/In_2S_3 photonaode.

of $TiO_2/CuInS_2(4)$-QDs/In_2S_3 photonaode, and their thickness is about ~1.3 μm. Figure 3b shows the high FESEM image (top view) magnifications and corresponding surface quantitative EDX analysis of $TiO_2/CuInS_2(4)$-QDs/In_2S_3 photonaode. It was found that there are few copper atoms and plenty of sulfur, indium atoms on the surface of $TiO_2/CuInS_2(4)$-QDs/In_2S_3 photonaode, indicating the existence of excess In_2S_3.

3.2. UV–Visible Absorption Property of $CuInS_2$-QDs/In_2S_3 Sensitized Photoanode. To investigate the suitability of $CuInS_2$-QDs/In_2S_3 for photovoltaic application, absorption studies were carried out. Figure 4 shows the absorption spectra

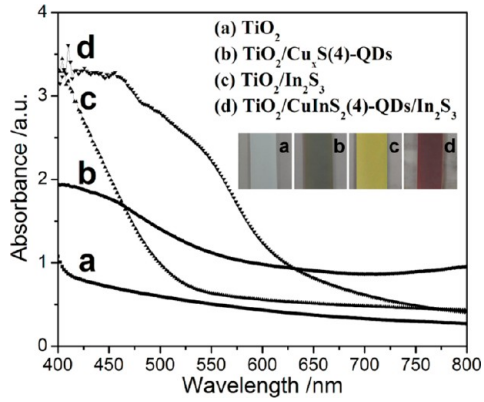

Figure 4. Optical absorption spectra of the plain nanocrystallineTiO_2 film, TiO_2/Cu_xS-QDs electrode prepared by four cycles of Cu_xS SILAR deposition, TiO_2/In_2S_3 electrode prepared by CBD of In_2S_3 for 3 h on the plain TiO_2 film, and $TiO_2/CuInS_2(4)$-QDs/In_2S_3 photonaode. The inset image shows the photographs of the corresponding electrodes.

of the correlative electrodes during the preparation process of $TiO_2/CuInS_2$-QDs/In_2S_3 photoanode from the plain TiO_2, TiO_2/Cu_xS-QDs to $TiO_2/CuInS_2$-QDs/In_2S_3 electrode. TiO_2/In_2S_3 electrode was chosen as a comparison. The spectrum shows that the plain TiO_2 can only absorb mainly UV light with wavelength smaller than 420 nm. The TiO_2/Cu_xS-QDs electrode can absorb UV to near-infrared light, but its optical absorptivity is rather weaker, and Cu_xS may vastly reduce solar cell performance. For the TiO_2 film with In_2S_3 CBD deposition, the light absorbance of the electrode was enhanced in the visible region, and its absorption band edge is about 530 nm. The prepared $TiO_2/CuInS_2$-QDs/In_2S_3 electrode has excellent optical adsorption performance not only in the UV region but also in the visible region. A shoulder appears between 525 and 650 nm with a long tail extending to longer wavelengths, which is mainly due to the formation of the $CuInS_2$ layer coated on the TiO_2 electrode. These results confirm that $CuInS_2$ layer can effectively improve the light absorption property of the TiO_2 film. In addition, the absorption of the $TiO_2/CuInS_2$-QDs/In_2S_3 electrode occurs at approximately 570 nm, and the absorption band edge is about 640 nm by a distinct blue-shift relative to that of bulk $CuInS_2$ (ca. 830 nm),[37] showing that the size of the $CuInS_2$ synthesized in this study is in the quantum confinement region. The inset image in Figure 4a shows the change in color of the TiO_2 electrodes after sensitization. The TiO_2 film was originally white and semi-transparent, becoming ash black when it was coated with Cu_xS QDs and maroon when it coated with $CuInS_2$-QDs/In_2S_3. Due to the quantum confinement effect in the optics, maroon color for the TiO_2/$CuInS_2$-QDs/In_2S_3 electrode is distinct from that of bulk $CuInS_2$.[37]

Figure 5 shows the absorption of the $TiO_2/CuInS_2$-QDs/In_2S_3 electrodes obtained by CBD of In_2S_3 and in situ reaction

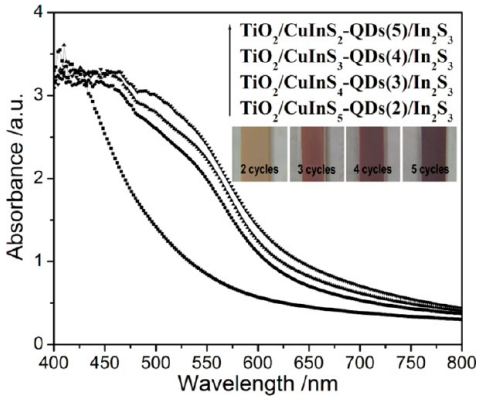

Figure 5. Optical absorption spectra of $TiO_2/CuInS_2$-QDs/In_2S_3 photonaodes obtained by CBD of In_2S_3 and in situ reaction with different cycles of Cu_xS SILAR deposition on TiO_2 films. The inset image shows the photographs of the corresponding electrodes.

with different cycles of Cu_xS SILAR deposition on TiO_2 film. When the Cu_xS SILAR cycles are less (below two cycles), the excess In_2S_3 may be covered on the surface of the TiO_2/$CuInS_2$-QDs/In_2S_3 photoanode, and its absorption spectrum is similar to that of the TiO_2/In_2S_3 electrode. The absorption spectra of the prepared $TiO_2/CuInS_2$-QDs/In_2S_3 photoanodes were red-shifted with the increase of the Cu_xS SILAR cycles probably because of the increase of $CuInS_2$-QDs size or the increase of $CuInS_2$-QDs layer thickness. The enhanced absorption in the longer wavelength region is due to the remission of quantum confinement effect on the $CuInS_2$ QDs.

3.3. Photovoltaic Performance of the Devices. Figure 6 shows the photocurrent−voltage characteristics (J−V curves) of

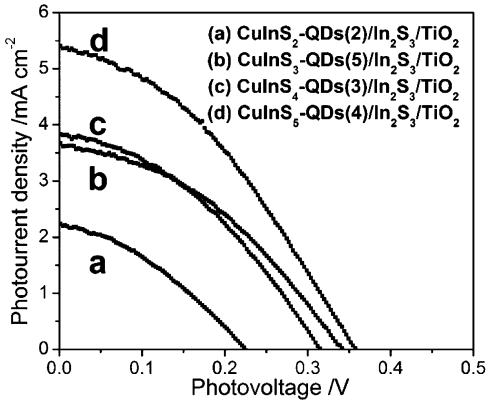

Figure 6. Photocurrent voltage characteristics of $TiO_2/CuInS_2$-QDs/In_2S_3 photonaodes obtained by CBD of In_2S_3 and in situ reaction with different cycles of Cu_xS SILAR deposition on TiO_2 films with Pt-FTO counter electrode.

the $TiO_2/CuInS_2$-QDs/In_2S_3 photonaodes with Pt-FTO CE, and the resultant photovoltaic parameters are summarized in Table 1. For the tested cell devices, with increasing the Cu_xS SILAR deposition from two cycles to four cycles, the short-circuit photocurrent (J_{sc}) and open-circuit photovoltage (V_{oc}) of $TiO_2/CuInS_2$-QDs/In_2S_3 photoanode increased substantially from 2.21 to 5.33 mA cm^{-2} and 0.22 to 0.36 V, respectively. The systematical increase of J_{sc} is attributed to extending the light absorption range and the increase in absorptivity with red-shift of the absorption onset of $CuInS_2$-QDs/In_2S_3 sensitizer, as shown in Figure 5. The increase of incorporated amount of

Table 1. Photovoltaic Parameters of $TiO_2/CuInS_2$-QDs/In_2S_3 Photonaodes Obtained by CBD of In_2S_3 and in Situ Reaction with Different Cycles of Cu_xS SILAR Deposition on TiO_2 Films with Pt-FTO Counter Electrode

photoanode	counter electrode	J_{sc} (mA cm^{-2})	V_{oc} (V)	*FF*	η (%)
$TiO_2/CuInS_2$(2)-QDs/In_2S_3	Pt-FTO	2.21	0.22	0.35	0.17
$TiO_2/CuInS_2$(3)-QDs/In_2S_3	Pt-FTO	3.81	0.31	0.38	0.46
$TiO_2/CuInS_2$(4)-QDs/In_2S_3	Pt-FTO	5.33	0.36	0.37	0.71
$TiO_2/CuInS_2$(5)-QDs/In_2S_3	Pt-FTO	3.62	0.34	0.39	0.48

$CuInS_2$-QDs can not only contribute to absorb more photons to generate more photoexcited electrons but also form a uniform and dense shell to reduce direct contact areas between the bare TiO_2 surface and polysulfide electrode, consequently decreasing the probability of recombination from separated electrons in the TiO_2 to the hole-transport material.[38,39] The QDSSc based four cycles Cu_xS SILAR deposition under our experimental conditions exhibit the optimum performance, with J_{sc} = 5.33 mA cm^{-2}, V_{oc} = 0.36 V, fill factor (*FF*) = 0.37, and η = 0.71%, respectively. However, the J_{sc}, V_{oc}, and η were found to decrease when the Cu_xS coating increased to five cycles. The possible reason for the reduced cell performance may be attributed to the aggregations and growth of the Cu_xS QDs, which will result in the presence of subsequently synthesized $CuInS_2$ QDs with no direct contact with the TiO_2, leading to higher recombination and thick sensitized layers blocking the infiltration of the electrolyte into the photoelectrode, thereby decreasing the regeneration efficiency of the solar cell.[40,41]

To improve the values of J_{sc}, V_{oc}, *FF*, and η of $TiO_2/CuInS_2$-QDs/In_2S_3 QDSSC, a Cu_2S-FTO CE was used. Figure 7 shows

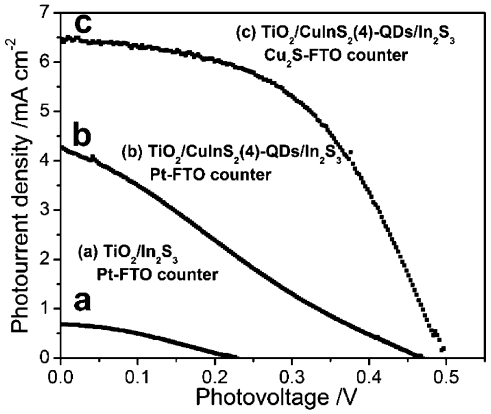

Figure 7. Photocurrent voltage characteristics of TiO_2/In_2S_3 (CBD for 3 h) and $TiO_2/CuInS_2$(4)-QDs/In_2S_3 electrodes with Pt-FTO or Cu_2S-FTO counter electrode.

the J−V curves of $TiO_2/CuInS_2$(4)-QDs/In_2S_3 electrodes with Pt-FTO or Cu_2S-FTO CE, and the resultant photovoltaic parameters are summarized in Table 2 (the TiO_2/In_2S_3 electrode prepared by CBD of In_2S_3 on TiO_2 film for 3 h was selected as an reference). The η of the TiO_2 or TiO_2/Cu_xS electrode was approximately zero (which is not displayed in Figure 7 and Table 2). The TiO_2/In_2S_3 electrode shows a poor photovoltaic performance, with J_{sc}= 0.69 mA cm^{-2} and η only

Table 2. Photovoltaic Parameters of TiO_2/In_2S_3 (CBD for 3 h) and $TiO_2/CuInS_2$(4)-QDs/In_2S_3 Electrodes with Pt-FTO or Cu_2S-FTO Counter Electrode

photoanode	counter electrode	J_{sc} (mA cm^{-2})	V_{oc} (V)	*FF*	η (%)
TiO_2/In_2S_3	Pt-FTO	0.69	0.23	0.34	0.053
$TiO_2/CuInS_2$(4)-QDs/In_2S_3	Pt-FTO	5.33	0.36	0.37	0.71
$TiO_2/CuInS_2$(4)-QDs/In_2S_3	Cu_2S-FTO	6.49	0.50	0.50	1.62

0.053. The as-prepared $TiO_2/CuInS_2$-QDs/In_2S_3 QDSSC featuring a Cu_2S-FTO electrode exhibits a better photovoltaic performance than that of Pt-FTO, with J_{sc} = 6.49 mA cm^{-2}, V_{oc} = 0.50 V, *FF* = 0.50, and η = 1.62%, respectively. The $TiO_2/CuInS_2$-QDs/In_2S_3 QDSSC shows better photovoltaic performance than that of the $TiO_2/CuInS_2$-QDs QDSSC reported by the literature.[15,16,19,20] TiO_2/In_2S_3 photoelectrdode has poor photovoltaic performance; therefore, we believe that $CuInS_2$-QDs are the main photo-sensitizers, and In_2S_3 may change the unmatched band alignments and high surface state density that exist in the heterostructure between TiO_2 and $CuInS_2$, which improves the cell performance. When employing a polysulfide electrolyte in QDSSCs, the commonly used Pt CE is only poorly active, mainly because its surface activity and conductivity are suppressed as a result of adsorption of the sulfur atom.[21]

To further reveal the reasons for the better electrochemical characteristics of Cu_2S-FTO CE compared to Pt-FTO CE, electrochemical impedance spectroscopy (EIS) experiments were performed with dummy cells fabricated with two identical electrodes (CE//electrolyte//CE). The test area was 0.36 cm^2. Figure 8 shows the corresponding equivalent circuit and the

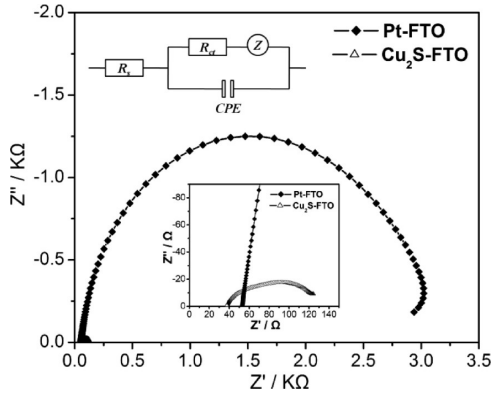

Figure 8. Nyquist plots of the dummy cell fabricated with two identical electrodes. The inset (above) displays the corresponding equivalent circuit; (below) the detailed plots in the high-frequency region.

detailed plots in the high-frequency region, where the high-frequency intercept on the real axis represents the ohmic series resistance (R_s). The maxima in the middle- and low-frequency regions arise from the charge-transfer resistance (R_{ct}), the corresponding constant phase angle element (CPE) at the CE/electrolyte interface,[42−45] and the Nernst diffusion impedance (Z) of the polysulfide electrolyte. The value of R_{ct} (Table 3) obtained by fitting the spectra in Figure 8 with an EIS spectrum analyzer, and it varies inversely with the electrochemical catalytic activity for the reduction of the polysulfide electrolyte.

Table 3. EIS Analysis Results of Symmetric Cells Using Pt-FTO and Cu_2S-FTO Counter Electrodes

counter electrode	R_s (Ω cm^2)	R_{ct} (Ω cm^2)	CPE
Pt-FTO	18.43	875.16	0.33
Cu_2S-FTO	12.54	36.22	0.15

From Table 3, it is observed that R_s (12.54 Ω cm^2) for Cu_2S-FTO CE is small, implying that the Cu_2S particles are firmly bonded to the FTO glass substrate. This can facilitate electron transmission across the Cu_2S/substrate interface. Interesting and importantly, Cu_2S-FTO CE exhibits the smaller R_{ct} (36.22 Ω cm^2), suggesting the higher electrochemical catalytic activity than Pt in polysulfide electrolyte.[34,46,47] This explains the high J_{sc} and *FF* of Cu_2S-FTO CE in *I*−*V* test.[21,35]

4. CONCLUSIONS

In this study, we have presented a facile SILAR process to deposit Cu_xS QDs on TiO_2 film, and then $CuInS_2$-QDs sensitized TiO_2 photoanodes with Cd-free In_2S_3 buffer layer were successfully prepared based on CBD of In_2S_3 and reaction with TiO_2/Cu_xS-QDs films. The well-connected In_2S_3 layer-like nets was found on the surface of the $TiO_2/CuInS_2$ photonaode. The absorption spectra of the prepared $TiO_2/CuInS_2$-QDs/In_2S_3 photoanodes were red-shifted with the increase of the Cu_xS SILAR cycles. On the basis of optimal Cu_xS SILAR cycles, the best photovoltaic performance with η of 1.62% (J_{sc} = 6.49 mA cm^{-2}, V_{oc} = 0.50 V, *FF* = 0.50) under full one-sun illumination was achieved by using Cu_2S on FTO glass CE. The Cu_2S electrode exhibits superior electro-catalytic ability for the polysulfide redox reactions relative to that of Pt electrode.

AUTHOR INFORMATION

Corresponding Authors

*Tel.: +86-21-67792881. Fax: +86-21-67792855. E-mail: wanghz@dhu.edu.cn (H. Z. Wang).

*E-mail: yaogang_li@dhu.edu.cn (Y. G. Li).

Notes

The authors declare no competing financial interest.

ACKNOWLEDGMENTS

We gratefully acknowledge the financial support by Natural Science Foundation of China (No. 51072034, 51172042), Specialized Research Fund for the Doctoral Program of Higher Education (20110075130001), Science and Technology Commission of Shanghai Municipality (12 nm0503900, 13JC1400200),the Program for Professor of Special Appointment (Eastern Scholar) at Shanghai Institutions of Higher Learning, Innovative Research Team in University (IRT1221), and the Program of Introducing Talents of Discipline to Universities (No.111-2-04).

REFERENCES

(1) David, R. B.; Prashant, V. K. *Adv. Funct. Mater.* **2009**, *19*, 805−811.

(2) Sun, W. T.; Yu, Y.; Pan, H. Y.; Gao, X. F.; Chen, Q.; Peng, L. M. *J. Am. Chem. Soc.* **2008**, *130*, 1124−1125.

(3) Bang, J. H.; Kamat, P. V. *Adv. Funct. Mater.* **2010**, *20*, 1970−1976.

(4) Wang, X. N.; Zhu, H. J.; Xu, Y. M.; Wang, H.; Tao, Y.; Hark, S.; Xiao, X. D.; Li, Q. A. *ACS Nano* **2010**, *4*, 3302−3308.

(5) Santhosh, K.; Samanta, A. *J. Phys. Chem. C* **2012**, *116*, 20643−20650.

(6) Sambur, J. B.; Novet, T.; Parkinson, B. *Science* **2010**, *330*, 63−66.

(7) Lee, H. J.; Leventis, H. C.; Moon, S. J.; Chen, P.; Ito, S.; Haque, S. A.; Torres, T.; Nüesch, F.; Geiger, T.; Zakeeruddin, S. M.; Grätzel, M.; Nazeeruddin, M. K. *Adv. Funct. Mater.* **2009**, *19*, 2735−2742.
(8) Yu, P. R.; Zhu, K.; Norman, A. G.; Ferrere, S.; Frank, A. J.; Nozik, A. J *J. Phys. Chem. B* **2006**, *110*, 25451−25454.
(9) Leweren, H. J.; Goslowsky, H.; Husemann, K. D.; Fiechter, S. *Nature* **1986**, *321*, 687−688.
(10) Landry, C. C.; Andrew, R. *Science* **1993**, *260*, 1653−1655.
(11) Nanu, M.; Schoonman, J.; Goossens, A. *Adv. Mater.* **2004**, *16*, 453−456.
(12) Kuo, K. T.; Liu, D. M.; Chen, S. Y.; Lin, C. C. *J. Mater. Chem.* **2009**, *19*, 6780−6788.
(13) Li, T. L.; Teng, H. S. *J. Mater. Chem.* **2010**, *20*, 3656−3664.
(14) Zhou, Z. J.; Fan, J. Q.; Wang, X.; Sun, W. Z.; Zhou, W. H.; Du, Z. L.; Wu, S. X. *Appl. Mater. Interfaces* **2011**, *3*, 2189−2194.
(15) Chang, J. Y.; Su, L. F.; Li, C. H.; Chang, C. C.; Lin, J. M. *Chem. Commun.* **2012**, *48*, 4848−4850.
(16) Li, T. L.; Lee, Y. L.; Teng, H. S. *Energy Environ. Sci.* **2012**, *5*, 5315−5324.
(17) Yang, Y. Y.; Zhang, Q. X.; Wang, T. Z.; Zhu, L. F.; Huang, X. M.; Zhang, Y. D.; Hu, X.; Li, D. M.; Luo, Y. H.; Meng, Q. B. *Electrochim. Acta* **2013**, *88*, 44−50.
(18) Santra, P. K.; Nair, P. V.; Thomas, K. G.; Kamat, P. V. *J. Phys. Chem. Lett.* **2013**, *4*, 722−729.
(19) Hu, X.; Zhang, Q. X.; Huang, X. M.; Li, D. M.; Luo, Y. H.; Luo, Y. H.; Meng, Q. B. *J. Mater. Chem.* **2011**, *21*, 15903−15905.
(20) Chang, J. Y.; Lin, J. M.; Su, L. F.; Chang, C. F. *ACS Appl. Mater. Interfaces* **2013**, *5*, 8740−8752.
(21) Hodes, G.; Manassen, J.; Cahen, D. *J. Electrochem. Soc.* **1980**, *127*, 544−549.
(22) Ruhle, S.; Yahav, S.; Greenwald, S.; Zaban, A. *J. Phys. Chem. C* **2012**, *116*, 17473−17478.
(23) Santra, P. K.; Kamat, P. V. *J. Am. Chem. Soc.* **2012**, *134*, 2508−2511.
(24) Zhang, H. Z.; Zhou, Y.; Ye, M.; He, Y. J.; He, C.; Yang, C. H.; Li, Y. F. *Chem. Mater.* **2008**, *20*, 6434−6443.
(25) Wang, D. S.; Zheng, W.; Hao, C. H.; Peng, Q.; Li, Y. D. *Chem. Commun.* **2008**, 2256−2558.
(26) Xie, R. G.; Rutherford, M.; Peng, X. G. *J. Am. Chem. Soc.* **2009**, *131*, 5691−5697.
(27) Xu, G. X.; Ji, S. L.; Miao, C. H.; Liu, G. D.; Ye, C. H. *J. Mater. Chem.* **2012**, *22*, 4890−4896.
(28) Chen, C.; Ali, G.; Yoo, S. H.; Kum, J. M.; Cho, S. O. *J. Mater. Chem.* **2011**, *21*, 16430−16435.
(29) Li, T. L.; Lee, Y. L.; Teng, H. S. *J. Mater. Chem.* **2011**, *21*, 5089−5098.
(30) Peng, Z. Y.; Liu, Y. L.; Shu, W.; Chen, K .Q.; Chen, W. *Eur. J. Inorg. Chem.* **2012**, 5239−5244.
(31) Prabhakar, R. R.; Pramana, S. S.; Karthik, K. R. G.; Sow, C. H.; Jinesh, K. B. *J. Mater. Chem.* **2012**, *22*, 13965−13968.
(32) Yella, A.; Lee, H. W.; Tsao, H. N.; Yi, C. Y.; Chandiran, A. K.; Nazeeruddin, M. K.; Diau, E. W. G.; Yeh, C. Y.; Zakeeruddin, S. M.; Grätzel, M. *Science* **2011**, *334*, 629−634.
(33) Bessho, T.; Zakeeruddin, S. M.; Yeh, C.; Diau, E. W. G.; Grätzel, M. *Angew. Chem., Int. Ed.* **2010**, *49*, 6646−6649.
(34) Gonzalez-Pedro, V.; Xu, X.; Mora-Sero, I.; Bisquert, J. *ACS Nano* **2010**, *4*, 5783−5790.
(35) Gimenez, S.; Mora-Sero, I.; Macor, L.; Guijarro, N.; Lana-Villarreal, T.; Gomez, R.; Diguna, L. J.; Shen, Q.; Toyoda, T.; Bisquert, J. *Nanotechnology* **2009**, *20*, 295204.
(36) Orphanou, M.; Leontidis, E.; Leodidou, T. K.; Koutsoukos, P.; Kyriacou, K. C. *Langmuir* **2004**, *20*, 5605−5612.
(37) Zhang, S. B.; Wei, S. H.; Zunger, A. *J. Appl. Phys.* **1998**, *83*, 3192−3197.
(38) Robel, I.; Subramanian, V.; Kuno, M.; Kamat, P. V. *J. Am. Chem. Soc.* **2006**, *128*, 2385−2393.
(39) Tang, Y. W.; Hu, X. Y.; Chen, M. J.; Luo, L. J.; Li, B. H.; Zhang, L. Z. *Electrochim. Acta* **2009**, *54*, 2742−2747.
(40) Wang, H.; Bai, Y S; Zhang, H.; Zhang, Z H; Li, J H; Guo, L. *J. Phys. Chem. C* **2010**, *114*, 16451−16455.
(41) Chen, H.; Fu, W. Y.; Yang, H. B.; Sun, P.; Zhang, Y. Y.; Wang, L. R.; Zhao, W. Y.; Zhou, X. M.; Zhao, H.; Jing, Q.; Qi, X. F.; Li, Y. X. *Electrochim. Acta* **2010**, *56*, 919−924.
(42) Li, K. X.; Luo, Y. H.; Yu, Z. X.; Deng, M. H.; Li, D. M.; Meng, Q. B. *Electrochem. Commun.* **2009**, *11*, 1346−1349.
(43) Wu, M. X.; Lin, X.; Hagfeldt, A.; Ma, T. L. *Angew. Chem., Int. Ed.* **2011**, *50*, 3520−3524.
(44) González-Pedro, V.; Xu, X.; Mora-Seró, I.; Bisquert, J. *ACS Nano* **2010**, *4*, 5783−5790.
(45) Kern, R.; Sastrawan, R.; Ferber, J.; Stangl, R.; Luther, J. *Electrochim. Acta* **2002**, *47*, 4213−4225.
(46) Radich, J. G.; Dwyer, R.; Kamat, P. V. *J. Phys. Chem. Lett.* **2011**, *2*, 2453−2460.
(47) Mora-Seró, I.; Giménez, S.; Moehl, T.; Fabregat-Santiago, F.; Lana-Villareal, T.; Gómez, R.; Bisquert, J. *Nanotechnology* **2008**, *19*, 424007.